
EVC-Net: Multi-scale V-Net with Conditional Random Fields for Brain Extraction

Jong Sung Park

Department of Intelligent Systems Engineering
 Indiana University
 Bloomington, IN 47405
 jp109@iu.edu

Shreyas Fadnavis

Department of Intelligent Systems Engineering
 Indiana University
 Bloomington, IN 47405
 shf.adn@iu.edu

Eleftherios Garyfallidis

Department of Intelligent Systems Engineering
 Indiana University
 Bloomington, IN 47405
 elef@iu.edu

Abstract

Brain extraction is one of the first steps of pre-processing 3D brain MRI data. It is a prerequisite for any forthcoming brain imaging analyses. However, it is not a simple segmentation problem due to the complex structure of the brain and human head. Although multiple solutions have been proposed in the literature, we are still far from having truly robust methods. While previous methods have used machine learning with structural/geometric priors, with the development of deep learning in computer vision tasks, there has been an increase in proposed convolutional neural network architectures for this semantic segmentation task. Yet, most models focus on improving the training data and loss functions with little change in the architecture. In this paper, we propose a novel architecture we call EVC-Net. EVC-Net adds lower scale inputs on each encoder block. This enhances the multi-scale scheme of the V-Net architecture, hence increasing the efficiency of the model. Conditional Random Fields, a popular approach for image segmentation before the deep learning era, are re-introduced here as an additional step for refining the network’s output to capture fine-grained results in segmentation. We compare our model to state-of-the-art methods such as HD-BET, Synthstrip and brainy. Results show that even with limited training resources, EVC-Net achieves higher Dice Coefficient and Jaccard Index along with lower surface distance.

1 Introduction

Brain MRI computes the tissue composition to create an image of the brain. However, other parts of the body also exist within the image. Unnecessary non-brain tissues could include face, eyes, spine, etc. For additional methods such as registration, tractography and tissue segmentation to work properly, it is important to have the image of the sole brain without other parts of the body that will

disrupt the algorithm or analysis. Accurate manual segmentation (gold-standard) can be ideal, but it is very time consuming with in need of an expert, who can also include biases in the results. Thus, automatic brain extraction, also called skull stripping is a semantic segmentation task necessary in pre-processing the brain in order to perform forthcoming analyses. Despite the simple explanation of the problem, difficulties rise from several factors of the MR images. Non-brain tissues are image-wise connected to the brain and have a very similar intensity compared to parts of the brain, especially white matter in T1 weighted images. This can create a common false positive in the algorithms. Artifacts and noise common in T1 weighted images can also disrupt the robustness of the methods.

Traditional machine learning methods for skull stripping have used information about the intensity, structure and templates of the MRI as a prior for the algorithm [9, 45, 46, 48]. While the methods have proven to give a reasonable segmentation mask of the brain, they often result in large error regions that have to be resolved by searching the parameter space or manually correcting them, which can take a very long time. Thus, there has been a large shift of the proposed methods to deep learning based models [6, 18, 20, 25, 34, 41].

Since the use of Alexnet [27] for image classification tasks, there have been many developments in using Deep Learning models for images [7, 15, 16]. However, there are several reasons why it is often not optimal to implement the model architecture and ideas directly to medical images. First, the lack of data. While it is relatively easy to acquire computer vision data that can come from various input devices, cameras, satellite images, videos etc, that is not the case for medical images. Since these contain personal information, it is difficult to gather the data in the first place and even harder to make the data public due to patient protection regulation and governmental guidelines. Hence, a lot of them cannot be used or shared among other research teams to train and evaluate their models on. Additionally, labeling the data demands careful analysis of the images by experts, thus there are fewer public data with true ground truth labels. Most ground truth labels provided in the public datasets are mainly created by another machine learning method with or without manual editing [14, 31, 38, 49]. The dimension of the data is another obstacle since most of the data are 3D, and even a single T1-weighted modality image is a few hundred computer vision images in size. The additional spatial dimension and the limit to complexity of the model from the heavy memory requirement creates complications in designing the model. Additionally, medical imaging data tends to have different properties (color channels, tasks, important features of the image, etc). This can limit the usage of some image augmentation techniques and complicate transfer learning, though these are both efficient tools when working with limited amount of training data.

Nevertheless, researchers have created efficient methods to improve deep learning models to work with medical images. Especially in segmentation tasks, while each model has it's unique characteristics, U-Net [40] and Cascade networks [44] have been the skeleton of most architecture types in the field. U-Net uses residual connection ideas with multiple layers of features using different scales to take account for features of various sizes. Cascade networks excludes unnecessary information from the image by first creating a mask using a coarse network, later using a finer network to get the exact results. Other methods have modified and enhanced these models, including but not limited to V-Net [36], 3D-UNet [4] and HD-BET [20]. While the various models have reached an overall good accuracy, there is still room for development in the architecture of the networks.

This paper aims to improve V-Net [36], a variant of U-Net. There are two major changes that V-Net suggests to the original U-Net architecture [40], additional residual connections and replacing max pooling layers with convolutional layers. However, it does not change the fact that the lower layer's information is limited to only the downsampled features from a higher scale layer. Also, the inevitable errors still occur from the imperfect training data labels. Our work suggests two ways to resolve these problems, multi-scale inputs and CRF.

2 Related work

2.1 Brain extraction

Despite the fact that multiple modalities can be used for brain extraction, in this paper we focus on T1 weighted brain MRI, as these are the most commonly used images for brain extraction and they are nearly always acquired with each scan.

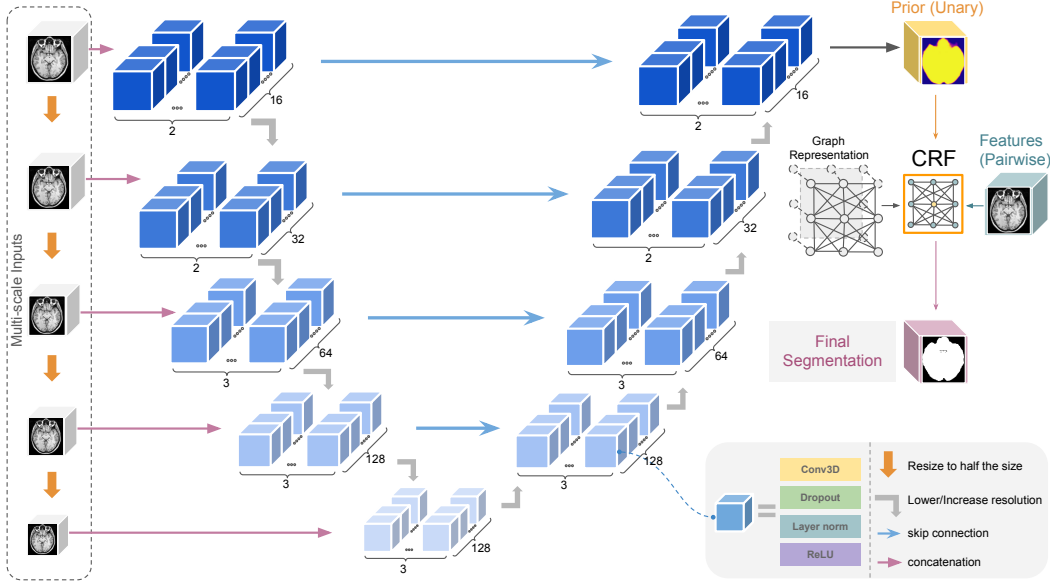


Figure 1: A summary of the architecture of proposed EVC-NET. Consists of three main components: 1) Multi-Scale inputs given to each level of the V-Net, 2) the V-Net which yields the initial segmentation given as unary potential to the CRF, and 3) the CRF itself which also takes a fully connected graph of voxels, pairwise potential and initial segmentation map to give the final refined output.

Traditional approaches in skull stripping use known priors of the brain. They can be categorized by what type of prior the algorithm relies on: morphology, intensity, surface structure, template matching or a combination of these [39]. While every method in any category have their ups and downs, we will discuss a few methods that are popularly used by experts and work on T1 weighted images. Rehman et al. [39] provides a good summary of the various methods proposed in the literature.

Brain Extraction Tool (BET) [48], one of the most used methods, uses the intensity and brain surface structure as its prior. It creates a initial sphere using the intensity differences per tissue type. The sphere is deformed on each direction to form the brain's shape. Even though the model is fast and does not need any pre-processing beforehand, it has been known to have its limitations in the segmentation results [1]. 3dSkullStrip used in Analysis of Functional NeuroImages (AFNI) [5] improves BET by adding a few modifications that helps exclude the eyes and the ventricles in the image, removing some of the false positive tissues. Ségonne et al. [45] adds an intensity/structure prior, using the fact that white matter has a higher intensity in the T1 modality and is one connected segment, to create an initial volume and later deforming it to match the brain surface. ROBEX (robust, learning-based brain extraction system) [19] uses a more hybrid approach of creating an initial mask by using a random forest classifier on extracted features, which is fit/deformed to match a more accurate surface.

Non-deformable suface based models are widely used as well. Brain Surface Extractor (BSE) uses anisotropic diffusion filters to smooth out low-contrast edges followed by edge detection with morphological erosion. The edges are later expanded to match the brain. BEaST [9] uses patchwise comparison to a set of templates pre-constructed from 80 segmented and manually corrected brain masks as a prior. It also uses multi-resolutions of patches to optimize the computation and reduce false negatives. ALFA (accurate learning with few atlases) [46] registers manually segmented neonatal brain atlases to the target image, selects the few closest to the average of them and fuses the labels using machine learning approaches to create the segmentation output.

Various deep learning approaches have been considered in brain extraction over the years [6, 18, 20, 25, 34, 41]. One of the major factors that characterize these models is the dimension the data is treated as. For deep learning models in brain extraction tasks, it might be troublesome when trying to train a model that stores all the full 3D features in memory. Most 2D convolutional network methods use 2D slices from all planes to get segmentations from each plane, later merging the results [17, 34, 41]. Dismantling the 3D image into smaller cubes has also been considered [25]. Other approaches

have cropped the image to a smaller size to use it as a form of augmentation as well [20, 22]. If using 3D image as a whole, decreasing the resolution of the input to a usable dimension has been suggested [21].

Models that work with damaged brains and multiple modalities have also been proposed. Brain-MaGe [50] was trained to be more specific to brains with tumors. HD-BET [20] was trained with brains with glioblastoma along with healthy subjects from public datasets to provide a generalized brain extraction method. Both were created to work with any of the 4 structural modalities. Synth-strip [18] created synthesized images by augmenting not just the image itself but on each part of the known whole-head anatomical segmentation. The fake images were used to train the model to be generalizable to any kind of human brain images.

While there are multiple types of architectures proposed in the literature, this paper will focus on one of the most utilized type of models, U-Net. The popularity of U-Net comes from its clever architecture of forcing the model to learn multi-scale features by using a max pooling layer for every block of layers and using an autoencoder like structure with skip connections. These skip connections between the encoder and decoder part of the model add an additional pass of information on each scale, making the model more segmentation friendly than simple autoencoders.

Since U-Net was introduced, many deep learning methods that train on medical images now use it as their base architecture [18, 20, 34, 41]. Though the original model was created for 2D medical image segmentation, there have been multiple models that modify this architecture to work for 3D [4, 36]. Other improvements have been introduced as well. Li et al. [32] added cascade networks to U-Net to help segmentation on data where the background might be significantly major than the foreground. W-Net [52] used two U-Net structures to do unsupervised segmentation of images. HD-BET [20] weighted the complexity of the model to be heavier in the encoder along with loss calculation per scale of the decoder part to facilitate training.

2.2 Conditional Random Fields

CRFs were originally used for segmenting and labeling sequence data [30]. The method is based on assuming the label's probability distribution to be a Markov Random Field (MRF). Various approaches have been conducted to use CRFs in image segmentation. The major difference in these methods is the initial segmentation algorithm for the prior distribution (probability of a pixel belonging to a certain label) and how the graph is constructed. Shotton et al. [47] used texture/color/spatial information to create an initial map with 4 neighboring pixels for the graph structure. Fulkerson et al. [11] created superpixels, a small group of pixels, and calculated the histogram of them to define the initial prior. Enhancing the CRF itself was also suggested using a hierarchical strategy [28, 29].

Krähenbühl and Koltun [26] suggested an efficient way of calculating CRFs so that the model could use a fully connected graph instead of just neighboring pairs. Their method uses the position and intensity information of the pixels to create an energy function, which is minimized to reduce the difference between the same labels. The initial segmentation is done by following the feature extraction concept from Shotton et al. [47]. We will explain more on the theorem behind their model.

Let us consider $X = X_1, X_2, \dots, X_N$ to be a vector of label assignments on each pixel 1 to N , where the value of each element is within the possibilities of label. In our case, since brain extraction is a binary segmentation problem, it would be either 0 or 1. Since we are assuming a MRF, it can be approximated as a Gibbs distribution with neighboring interactions. Thus, given image I , we can write a Gibbs distribution $P(X = x|I) = \frac{\exp(-E(x|I))}{Z(I)}$. $Z(I)$ is the denominator dependent on only the image itself, so can be ignored. The model aims to find the maximum x that has the highest probability, thus the lowest energy function. Krähenbühl and Koltun [26] defines the Gibbs energy as

$$E(x) = \sum_i \psi_u(x_i) + \sum_{i < j} \psi_p(x_i, x_j)$$

where ψ_u is the unary potential (potential of a single pixel/voxel) and ψ_p is the pairwise potential (potential from its neighboring information). Note that the dependency on the image I was omitted for convenience. In our case, the unary potential will be our deep learning model's output. The pairwise potential is defined as

$$\psi_p(x_i, x_j) = \mu(x_i, x_j) \sum_{m=1}^K w^{(m)} k^{(m)}(f_i, f_j)$$

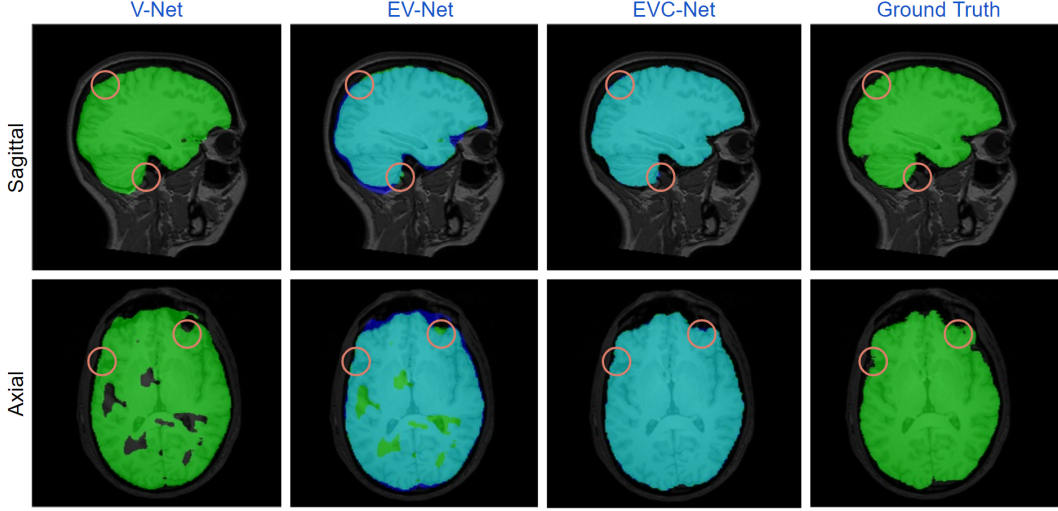


Figure 2: Depicts results of the model output from V-Net, EV-Net and EVC-Net with the ground truth. Note that there are significant improvements from V-Net to EV-Net, while EVC-Net further captures finer details in the cerebellum and gyri of the brain. Green region represents the current model’s output and blue region the previous model’s output. Teal indicates the overlapping region.

where μ is the compatibility function that serves as penalty between different labels with similar features and $k^{(m)}$ is the kernel that utilizes feature f_i, f_j information. The paper uses position (smoothness) and intensity/position (appearance) kernels as the feature information. They are defined below.

$$k(f_i, f_j) = w^{(1)} \exp\left(-\frac{|p_i - p_j|^2}{2\theta_\alpha^2} - \frac{|I_i - I_j|^2}{2\theta_\beta^2}\right) + w^{(2)} \exp\left(-\frac{|p_i - p_j|^2}{2\theta_\gamma^2}\right)$$

p_i and I_i are each the spatial and intensity information of pixel i. $\theta_\alpha, \theta_\beta, \theta_\gamma$ controls the degree of each feature.

They also provide a way of efficiently approximating the posterior distribution (essentially the probability map) using mean field approximation. A quick summary of the method is described here. It assumes an independent relationship between the latent variables, in our case the true labels of each pixel/voxel. Since our goal is to find the most accurate approximation of the posterior, we can aim to find the minimum KL-Divergence between the posterior and the approximation. Through Bayesian inference one can calculate that the prior is a sum of the KL-Divergence and negative variational free energy. Krähenbühl and Koltun [26] showed that this can be written in the form of the unary potential and the pairwise potential. The assumption on the independence of the latent variables lets each variable to be updated separately treating the other variables as constants. Thus, each iteration of latent variable update that increases the negative variational free energy is guaranteed to decrease the KL-Divergence. Optimally, the converged output would be the true segmentation probability map of the image. Details on the method can be found in Krähenbühl and Koltun [26].

Deep Learning model’s image segmentation output is mainly a softmax result of the final layer. Since this gives a probability distribution of a pixel belonging to a certain label, using CRFs after a deep learning model would be a good way of improving the final result without further optimizing the model. Zheng et al. [54] integrated the iteration process from Krähenbühl and Koltun [26] as a Recurrent Layer. Unlike the original fully connected CRF model[26] including the CRF process in the model architecture itself also reduces the number of hyperparameters. While both the manual and Recurrent Layer approaches have been utilized in many medical imaging domains, [8, 10, 23, 33, 35, 51], Monteiro et al. [37] have suggested that using CRF as Recurrent Layer within the deep learning architecture does not help much with the volumetric segmentation.

3 Methods

Due to the size and complexity of brain MRI and lack of public data, it is important to have an efficient model that works with limited resources. This paper will propose two ways to enhance deep learning architectures for brain extraction, multi-scale inputs for efficiency of the model and Conditional Random Fields to get a finer segmentation result. The overall architecture is shown in Fig. 1.

3.1 EV-Net

We first propose EV-Net, which further improves the efficient multi-scale usage of information along with additional improvements in the V-Net [36] model. The major improvement comes from concatenating lower scale inputs to the output of each downsampling convolutional layer, which creates an 'E' like shape. (Note: Other minor changes of the model from the original proposed V-Net[36] can be found in the supplementary section.)

We can write a general equation for the output of a layer in the model as

$$y = \sigma(z)$$

$$z = wx + b$$

where w is the weight, x is the input, b is the bias and σ is any non-linear function. The gradient of w is calculated through backpropagation to update the weight (kernel in convolutional layers). By the chain rule, we know that the gradient value is a multiplication of the gradients of the deeper layers, the non-linear function and the input to the current layer. We can write this as

$$\frac{\delta L}{\delta w} = G \frac{\delta x'}{\delta z} \frac{\delta z}{\delta w}$$

where L is the loss function, G is the previous gradients in the chain rule, x' is the input to the next layer. There are two major changes one can make in the layer to modify the target gradient. One is altering the non-linear function, hence changing $\frac{\delta x'}{\delta z}$. We aim to change $\frac{\delta z}{\delta w}$ which is the input to the layer. In other words, we are defining x to be

$$x = x_{prev} + x_{raw}$$

x_{prev} stands for the input from the previous layer that reduces the feature size. This is present in any U-Net type architecture. x_{raw} is the raw input resized to match the layer's feature shape. It forces the weight to update using a meaningful information even if the x_{prev} provides a non-important feature, which is the case when training from a randomly initialized model. This multi-scale scheme is especially helpful in medical imaging segmentation, as transfer learning is often not an option.

3.2 Refinement of segmentation using CRFs

While the results of EV-Net are performing well, there is still space to improve. We need the final brain labels to follow the complex, intricate and detailed structure of the brain. A lot of features are considered when calculating a brain mask, but one cannot deny the fact that continuity in intensity and structure is an important factor. As CRFs are known to minimize the discrepancies in labels between neighboring pixels with similar intensity and spatial information, they can be used to create a fine-grained segmentation result. Even though the level of accuracy can be reached without it, greater training resources are required to learn the details. Although popularly used, adding CRF as a Recurrent Layer was not selected as it is not known to have a huge effect in volumetric medical image segmentation [37]. While there are other optimization methods for CRF proposed in medical images [35], we follow the method suggested in Krähenbühl and Koltun [26] for efficiency. Implementations revised to work with 3D image segmentation by Kamnitsas et al. [23] were used.

Additional processing: To remove small segmentation errors that might be present in the result, only the largest background segment was considered a background. Then, as the optimal brain extraction will naturally give a single connected cluster only, the largest connected foreground segment was used.

3.3 Training details

EVC-Net was trained using two Tesla V100s for 18 epochs. V-Net and EV-Net were trained with the same hardware and training conditions. The EV-Net and EVC-Net share the architecture and parameters of V-Net in most aspects except from the multi-scale inputs and CRF updates. They are summarized in Fig. 2. More details on the training environment and the exact parameters for CRF can be found in supplementary materials.

4 Results

1438 T1 MR images were used for training from the following datasets: the Human Connectome Project(HCP) [14], CC359 [49] and NFBs [38]. The images were first transformed to the RAS+ coordinate space with voxel resolution of $1\text{mm} \times 1\text{mm} \times 1\text{mm}$ by using the affine matrix given with the image file to match the resolution in each image. The images were then padded to a shape of (256, 256, 256) and resized to (128, 128, 128) to keep the resolution constant (now 2mm per each voxel dimension) while having an identical shape necessary for deep learning models. The provided labels of the datasets were used for training. For testing purposes, 6 images from the IXI dataset [3] were used. The labels were created by first running BET [48], then ITK-SNAP [53] and DIPY Horizon[12, 13] was used for manually correcting the errors.

Augmentation has been known to force the model to learn structural components. It is particularly important for medical images due to the lack of data. For intensity augmentation, we have used scaling and shifting of values to add random noise. For transformation augmentation, rotation and translation were used. This was to compensate for most of the minor differences T1 weighted images might have when in the same coordinate space. Augmentation was performed randomly on the training data each time it was loaded to improve generality without increasing the size of the training dataset.

Evaluation between models was done with three metrics. Dice Coefficient and Jaccard Index were selected to measure the similarity of the prediction to the ground truth. While both are used for evaluation of image segmentation, Dice Coefficient adds more weight to the True Positives than Jaccard Index. Aydin et al. [2] suggests an error exists in ranking segmentation results using Average Hausdorff Distance, due to the inconsistency in the segment size between predictions that is used as one of the denominators. They provide a balanced version of the equation they call Balanced Average Hausdorff Distance, which replaces the prediction segment size with the ground truth segment size for consistency. Therefore we chose Balanced Average Hausdorff Distance to measure a more stable average surface distance error.

4.1 Comparisons within model improvements

We first compare results from V-Net [36], EV-Net and EVC-Net to show the development of results per each change in the model. Fig. 2 shows the results in a single image in the evaluation dataset on different slices. Ground truth image is also provided in the figure for overall performance evaluation.

Each improvement (multi-scale input and the CRF layer) of the architecture corresponds to improvement of accuracy. We would like to emphasize that the training epochs of V-Net and EV-Net were exactly the same, without a single change in parameters except the addition of multi-scale inputs. Thus, the increase in accuracy would have been purely from the improvement of the model architecture. The additional inputs would have provided meaningful features from the low scale input for early training for EV-Net. For EVC-Net, CRFs added more details to the segmentation by escaping inevitable bias in the training set as they are more reliant to the information of the input image than the deep learning model. The original V-Net however would suffer from these issues, resulting in low performance of the model as seen in Fig. 2.

Also note that our model is considerably competent compared to other architectures as well. The models were trained on maximum 18 epochs with 1438 images, while for example, HD-BET [20] uses about 3000 images and trains for 200 epochs. The convergence speed is very promising and reinforces our argument on the effect of multi-scale inputs.

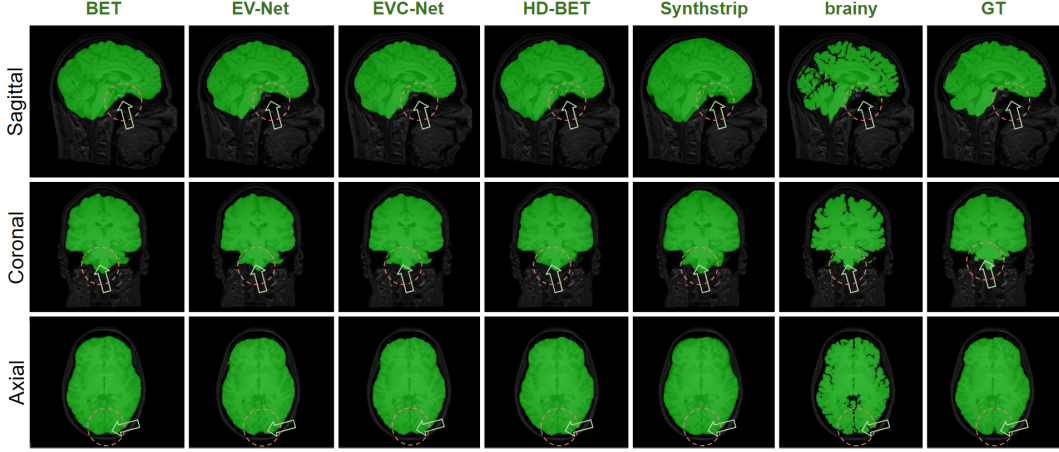


Figure 3: Results showing qualitative comparisons of different models with respect to the ground truth. Differences in detail of the segmentation results are pointed out. While the models look similar to each other, they have subtle discrepancies leading to differences in accuracy.

Table 1: Metrics evaluated on the test dataset between the compared models

| Model | Dice score | Jaccard Index | Surface Distance |
|-------------------------|----------------------------|----------------------------|-------------------------|
| BET [48] | 0.9620 \pm 0.0081 | 0.9268 \pm 0.1515 | 21.35 \pm 3.72 |
| EV-Net | 0.9674 \pm 0.0031 | 0.9370 \pm 0.0057 | 16.87 \pm 2.29 |
| EVC-Net | 0.9677 \pm 0.0032 | 0.9374 \pm 0.0061 | 16.96 \pm 2.20 |
| HD-BET [20] | 0.9674 \pm 0.0064 | 0.9370 \pm 0.0120 | 20.86 \pm 2.77 |
| Nobrainer (brainy) [22] | 0.9273 \pm 0.0081 | 0.8646 \pm 0.0140 | 39.12 \pm 1.86 |
| Synthstrip [18] | 0.9383 \pm 0.0094 | 0.8840 \pm 0.0168 | 21.06 \pm 1.78 |

4.2 Comparison with other models

We also compare our EVC-Net to other publicly available models. Fig. 3 show the results of each model on several images. Table 1 shows the average of each metric on the test dataset. BET was selected for comparison as it is the state-of-the-art non-deeplearning algorithms and they have been used for evaluation in multiple papers [18, 20]. The deep learning models [18, 20, 22] were selected based on whether they were publicly available for usage and known to work on T1 images of normal brains. EV-Net was included to show the enhancement of the model.

As seen in Table 1, EVC-Net out scored the other models in spatial overlap accuracy, provided by the Dice Score and Jaccard Index. This is expected as the model is designed to catch more detailed segments of the image effectively. However, EV-Net achieved the lowest surface distance. We believe this to be a result from an amplification of error of the CRF. CRF heavily depends on its unary potential (the provided initial segmentation). Therefore, if the segmentation had a relatively large portion of non-brain tissues with a similar surrounding intensity, it would lean towards increasing the error portion. Since these tend to be an outlying region, it could have a greater effect on surface distance than region wise accuracy.

Differences in ground truth An interesting observation here is the large difference in segmentation results between Synthstrip [18] and our method. Also, Synthstrip has lower metrics than the results provided in their paper on the same dataset. We believe this to be from how the ground truth is defined. While the ground truth provided by us focuses more on catching details of the brain structure, the ground truths used in Synthstrip’s evaluation focused more on a smoothed atlas structure of the brain. The comparison is provided in the supplementary material.

5 Discussion (Limitations and Future work)

Despite our model’s performance in the evaluation dataset, it is limited to non-pathological T1 weighted MRI data unlike other proposed methods [18, 20, 50]. However, we believe when provided with enough variety in images, the model would be able to train up to a state where it can provide output for abnormal brains, as the model utilizes raw low scale data, which can be useful for a less over-fitted segmentation. CRF will also provide correction to errors that could be caused by the lack of abnormal brain data. Further work would be extending the dataset for general use by adding more variety in modalities or clinical cases of the training data.

Since the CRF model proposed by Krähenbühl and Koltun [26] was created for computer vision tasks, the feature space it considers for the pairwise potential is relatively small on 3D gray scale images. This could be the reason for the little effect the CRF Recurrent Layer had on 3D medical image segmentation reported in Monteiro et al. [37]. Iglesias et al. [19] suggests using edge magnitude and derivative of gaussians for features of the voxels in the brain MRI, which could be used as an alternative pairwise potential, letting the CRF perform at its full potential. Also, improving the model for the initial segmentation can be crucial to its performance, since the results heavily depend on the initial probability map.

We provide a general enhancement that could be added to any U-Net type architecture, but the evaluation is done only on a skull stripping task. Nevertheless, due to the nature of the model, we believe this could also work on other medical image segmentation tasks that require fine-grained outputs. Brain tissue segmentation is a good candidate, where the goal is to segment the brain into white matter, gray matter and the CSF portion. The intensity differences of the each tissue is utilizable by CRF. Each segment has unique low and high scale features, thus can benefit from the multi-scale inputs by directly providing them to the deeper layers. Similar approaches can be used for other medical image segmentation tasks such as tumor segmentation. It is also reasonable to assume that the model could work with other modalities of structural MRI.

The paper emphasizes on the enhancement of the overall architecture, but there are still other changes for fine tuning the model for potentially better performance. For instance, Instance Normalization was proposed in StyleGAN [24] and had cases where it performed reasonably well in medical imaging tasks [43]. Many losses have been proposed as alternatives to dice loss which we would like to test in the future [18, 42].

6 Conclusion

Removing non-brain tissues from MRI data is a necessary step for nearly all forthcoming analyses of these images. Various deep learning approaches have been considered in the literature. However, most of their model architectures have little difference to the popularly used U-Net. Here we propose EVC-Net as an improvement to the base architecture of deep learning models for 3D brain extraction. Results show that adding multi-scale inputs of the raw-data and adding CRFs for refining the segmentation results can improve the output. We also show that this simple architectural change can result in a high accuracy with very high training efficiency (less training resources required). We think it is exciting and refreshing for the scientific community that a simple improvement to the model and a revisit to CRFs in medical imaging can be used in tandem, creating a compound effect, further improving crucial medical imaging segmentation problems such as skull stripping. A unit-tested version of the code will be open sourced via DIPY [12] to disseminate its use to the wider community.

Broader Impacts The research provides broader impacts on improvements on overall medical image segmentation methods that use U-Net/V-Net type architectures utilizing multi-scale inputs and CRFs. Accurate segmentation of Regions of Interest is crucial in medical images for the best performance of additional analysis, allowing more accurate measures of the target features. Our method provides not only accuracy but efficiency improvements as well. Therefore, in theory ECV-Net could potentially be a good base architecture for many other semantic segmentation models.

EVC-Net provides an efficient and accurate way of medical image segmentation. As with all deep learning approaches, despite the relative efficiency of the model, has a high carbon footprint due to the memory and computation resources used. The heavy amount of necessary calculation of deep learning can also increase the gap between researchers with and without the required assets. However,

research towards efficient models provides a step towards reducing the energy consumption and reducing model complexity.

References

- [1] M Stella Atkins, Kevin Siu, Benjamin Law, Jeffery J Orchard, and Wilfred L Rosenbaum. Difficulties of t1 brain mri segmentation techniques. In *Medical Imaging 2002: Image Processing*, volume 4684, pages 1837–1844. SPIE, 2002.
- [2] Orhun Utku Aydin, Abdel Aziz Taha, Adam Hilbert, Ahmed A Khalil, Ivana Galinovic, Jochen B Fiebach, Dietmar Frey, and Vince Istvan Madai. On the usage of average hausdorff distance for segmentation performance assessment: hidden error when used for ranking. *European Radiology Experimental*, 5(1):1–7, 2021.
- [3] brain-development.org team. Ixi dataset. URL <https://brain-development.org/ixi-dataset/>. [Online; accessed 2-May-2022].
- [4] Özgün Çiçek, Ahmed Abdulkadir, Soeren S Lienkamp, Thomas Brox, and Olaf Ronneberger. 3d u-net: learning dense volumetric segmentation from sparse annotation. In *International conference on medical image computing and computer-assisted intervention*, pages 424–432. Springer, 2016.
- [5] Robert W Cox. Afni: what a long strange trip it’s been. *Neuroimage*, 62(2):743–747, 2012.
- [6] Raunak Dey and Yi Hong. Compnet: Complementary segmentation network for brain mri extraction. In *International Conference on Medical Image Computing and Computer-Assisted Intervention*, pages 628–636. Springer, 2018.
- [7] Alexey Dosovitskiy, Lucas Beyer, Alexander Kolesnikov, Dirk Weissenborn, Xiaohua Zhai, Thomas Unterthiner, Mostafa Dehghani, Matthias Minderer, Georg Heigold, Sylvain Gelly, et al. An image is worth 16x16 words: Transformers for image recognition at scale. *arXiv preprint arXiv:2010.11929*, 2020.
- [8] Nguyen Ho Minh Duy, Nguyen Manh Duy, Mai Thanh Nhat Truong, et al. Accurate brain extraction using active shape model and convolutional neural networks. 2018.
- [9] Simon F Eskildsen, Pierrick Coupé, Vladimir Fonov, José V Manjón, Kelvin K Leung, Nicolas Guizard, Shafik N Wassef, Lasse Riis Østergaard, D Louis Collins, Alzheimer’s Disease Neuroimaging Initiative, et al. Beast: brain extraction based on nonlocal segmentation technique. *NeuroImage*, 59(3):2362–2373, 2012.
- [10] Huazhu Fu, Yanwu Xu, Stephen Lin, Damon Wing Kee Wong, and Jiang Liu. Deepvessel: Retinal vessel segmentation via deep learning and conditional random field. In *International conference on medical image computing and computer-assisted intervention*, pages 132–139. Springer, 2016.
- [11] Brian Fulkerson, Andrea Vedaldi, and Stefano Soatto. Class segmentation and object localization with superpixel neighborhoods. In *2009 IEEE 12th international conference on computer vision*, pages 670–677. IEEE, 2009.
- [12] Eleftherios Garyfallidis, Matthew Brett, Bagrat Amirbekian, Ariel Rokem, Stefan Van Der Walt, Maxime Descoteaux, Ian Nimmo-Smith, and Dipy Contributors. Dipy, a library for the analysis of diffusion mri data. *Frontiers in neuroinformatics*, 8:8, 2014.
- [13] Eleftherios Garyfallidis, Serge Koudoro, Javier Guaje, Marc-Alexandre Côté, Soham Biswas, David Reagan, Nasim Anousheh, Filipi Silva, Geoffrey Fox, and Fury Contributors. Fury: advanced scientific visualization. *Journal of Open Source Software*, 6(64):3384, 2021. doi: 10.21105/joss.03384. URL <https://doi.org/10.21105/joss.03384>.
- [14] Matthew F Glasser, Stamatios N Sotiroopoulos, J Anthony Wilson, Timothy S Coalson, Bruce Fischl, Jesper L Andersson, Junqian Xu, Saad Jbabdi, Matthew Webster, Jonathan R Polimeni, et al. The minimal preprocessing pipelines for the human connectome project. *Neuroimage*, 80: 105–124, 2013.

[15] Ian Goodfellow, Jean Pouget-Abadie, Mehdi Mirza, Bing Xu, David Warde-Farley, Sherjil Ozair, Aaron Courville, and Yoshua Bengio. Generative adversarial nets. *Advances in neural information processing systems*, 27, 2014.

[16] Kaiming He, Georgia Gkioxari, Piotr Dollár, and Ross Girshick. Mask r-cnn. In *Proceedings of the IEEE international conference on computer vision*, pages 2961–2969, 2017.

[17] Leonie Henschel, Sailesh Conjeti, Santiago Estrada, Kersten Diers, Bruce Fischl, and Martin Reuter. Fastsurfer-a fast and accurate deep learning based neuroimaging pipeline. *NeuroImage*, 219:117012, 2020.

[18] Andrew Hoopes, Jocelyn S Mora, Adrian V Dalca, Bruce Fischl, and Malte Hoffmann. Synth-strip: Skull-stripping for any brain image. *arXiv preprint arXiv:2203.09974*, 2022.

[19] Juan Eugenio Iglesias, Cheng-Yi Liu, Paul M Thompson, and Zhuowen Tu. Robust brain extraction across datasets and comparison with publicly available methods. *IEEE transactions on medical imaging*, 30(9):1617–1634, 2011.

[20] Fabian Isensee, Marianne Schell, Irada Pflueger, Gianluca Brugnara, David Bonekamp, Ulf Neuberger, Antje Wick, Heinz-Peter Schlemmer, Sabine Heiland, Wolfgang Wick, et al. Automated brain extraction of multisequence mri using artificial neural networks. *Human brain mapping*, 40(17):4952–4964, 2019.

[21] Ivan Itzcovich. Deepbrain. <https://github.com/iitzco/deepbrain>, 2018.

[22] Jakub Kaczmarzyk, Patrick McClure, Wazeer Zulfikar, Aakanksha Rana, Hoda Rajaei, Adam Richie-Halford, Shashank Bansal, Dorota Jarecka, John Lee, and Satrajit Ghosh. neu-ronets/nobrainer: 0.3.0, 2022. URL <https://zenodo.org/record/4995077>.

[23] Konstantinos Kamnitsas, Christian Ledig, Virginia FJ Newcombe, Joanna P Simpson, Andrew D Kane, David K Menon, Daniel Rueckert, and Ben Glocker. Efficient multi-scale 3d cnn with fully connected crf for accurate brain lesion segmentation. *Medical image analysis*, 36:61–78, 2017.

[24] Tero Karras, Samuli Laine, and Timo Aila. A style-based generator architecture for generative adversarial networks. In *Proceedings of the IEEE/CVF conference on computer vision and pattern recognition*, pages 4401–4410, 2019.

[25] Jens Kleesiek, Gregor Urban, Alexander Hubert, Daniel Schwarz, Klaus Maier-Hein, Martin Bendszus, and Armin Biller. Deep mri brain extraction: A 3d convolutional neural network for skull stripping. *NeuroImage*, 129:460–469, 2016.

[26] Philipp Krähenbühl and Vladlen Koltun. Efficient inference in fully connected crfs with gaussian edge potentials. *Advances in neural information processing systems*, 24, 2011.

[27] Alex Krizhevsky, Ilya Sutskever, and Geoffrey E Hinton. Imagenet classification with deep convolutional neural networks. *Advances in neural information processing systems*, 25, 2012.

[28] Sanjiv Kumar and Martial Hebert. A hierarchical field framework for unified context-based classification. In *Tenth IEEE International Conference on Computer Vision (ICCV'05) Volume 1*, volume 2, pages 1284–1291. IEEE, 2005.

[29] L'ubor Ladický, Chris Russell, Pushmeet Kohli, and Philip HS Torr. Associative hierarchical crfs for object class image segmentation. In *2009 IEEE 12th International Conference on Computer Vision*, pages 739–746. IEEE, 2009.

[30] John Lafferty, Andrew McCallum, and Fernando CN Pereira. Conditional random fields: Probabilistic models for segmenting and labeling sequence data. 2001.

[31] Pamela J LaMontagne, Tammie LS Benzinger, John C Morris, Sarah Keefe, Russ Hornbeck, Chengjie Xiong, Elizabeth Grant, Jason Hassenstab, Krista Moulder, Andrei G Vlassenko, et al. Oasis-3: longitudinal neuroimaging, clinical, and cognitive dataset for normal aging and alzheimer disease. *MedRxiv*, 2019.

[32] Suiyi Li, Yuxuan Chen, Su Yang, and Wuyang Luo. Cascade dense-unet for prostate segmentation in mr images. In *International Conference on Intelligent Computing*, pages 481–490. Springer, 2019.

[33] Yi Li and Wei Ping. Cancer metastasis detection with neural conditional random field. *arXiv preprint arXiv:1806.07064*, 2018.

[34] Oeslle Lucena, Roberto Souza, Leticia Rittner, Richard Frayne, and Roberto Lotufo. Convolutional neural networks for skull-stripping in brain mr imaging using silver standard masks. *Artificial intelligence in medicine*, 98:48–58, 2019.

[35] Chris S Magnano, Ameet Soni, Sriraam Natarajan, and Gautam Kunapuli. Conditional random fields for brain tissue segmentation. In *Proc. SDM*, 2014.

[36] Fausto Milletari, Nassir Navab, and Seyed-Ahmad Ahmadi. V-net: Fully convolutional neural networks for volumetric medical image segmentation. In *2016 fourth international conference on 3D vision (3DV)*, pages 565–571. IEEE, 2016.

[37] Miguel Monteiro, Mário AT Figueiredo, and Arlindo L Oliveira. Conditional random fields as recurrent neural networks for 3d medical imaging segmentation. *arXiv preprint arXiv:1807.07464*, 2018.

[38] Benjamin Puccio, James P Pooley, John S Pellman, Elise C Taverna, and R Cameron Craddock. The preprocessed connectomes project repository of manually corrected skull-stripped t1-weighted anatomical mri data. *Gigascience*, 5(1):s13742–016, 2016.

[39] Hafiz Zia Ur Rehman, Hyunho Hwang, and Sungon Lee. Conventional and deep learning methods for skull stripping in brain mri. *Applied Sciences*, 10(5):1773, 2020.

[40] Olaf Ronneberger, Philipp Fischer, and Thomas Brox. U-net: Convolutional networks for biomedical image segmentation. In *International Conference on Medical image computing and computer-assisted intervention*, pages 234–241. Springer, 2015.

[41] Seyed Sadegh Mohseni Salehi, Deniz Erdogmus, and Ali Gholipour. Auto-context convolutional neural network (auto-net) for brain extraction in magnetic resonance imaging. *IEEE transactions on medical imaging*, 36(11):2319–2330, 2017.

[42] Seyed Sadegh Mohseni Salehi, Deniz Erdogmus, and Ali Gholipour. Tversky loss function for image segmentation using 3d fully convolutional deep networks. In *International workshop on machine learning in medical imaging*, pages 379–387. Springer, 2017.

[43] Kurt G Schilling, Justin Blaber, Yuankai Huo, Allen Newton, Colin Hansen, Vishwesh Nath, Andrea T Shafer, Owen Williams, Susan M Resnick, Baxter Rogers, et al. Synthesized b0 for diffusion distortion correction (synb0-disco). *Magnetic resonance imaging*, 64:62–70, 2019.

[44] Jo Schlemper, Jose Caballero, Joseph V Hajnal, Anthony N Price, and Daniel Rueckert. A deep cascade of convolutional neural networks for dynamic mr image reconstruction. *IEEE transactions on Medical Imaging*, 37(2):491–503, 2017.

[45] Florent Ségonne, Anders M Dale, Evelina Busa, Maureen Glessner, David Salat, Horst K Hahn, and Bruce Fischl. A hybrid approach to the skull stripping problem in mri. *Neuroimage*, 22(3):1060–1075, 2004.

[46] Ahmed Serag, Manuel Blesa, Emma J Moore, Rozalia Pataky, Sarah A Sparrow, AG Wilkinson, Gillian Macnaught, Scott I Semple, and James P Boardman. Accurate learning with few atlases (alfa): an algorithm for mri neonatal brain extraction and comparison with 11 publicly available methods. *Scientific Reports*, 6(1):1–15, 2016.

[47] Jamie Shotton, John Winn, Carsten Rother, and Antonio Criminisi. Textonboost for image understanding: Multi-class object recognition and segmentation by jointly modeling texture, layout, and context. *International journal of computer vision*, 81(1):2–23, 2009.

[48] Stephen M Smith. Fast robust automated brain extraction. *Human brain mapping*, 17(3):143–155, 2002.

- [49] Roberto Souza, Oeslle Lucena, Julia Garrafa, David Gobbi, Marina Saluzzi, Simone Appenzeller, Letícia Rittner, Richard Frayne, and Roberto Lotufo. An open, multi-vendor, multi-field-strength brain mr dataset and analysis of publicly available skull stripping methods agreement. *NeuroImage*, 170:482–494, 2018.
- [50] Siddhesh Thakur, Jimit Doshi, Sarthak Pati, Saima Rathore, Chiharu Sako, Michel Bilello, Sung Min Ha, Gaurav Shukla, Adam Flanders, Aikaterini Kotrotsou, et al. Brain extraction on mri scans in presence of diffuse glioma: Multi-institutional performance evaluation of deep learning methods and robust modality-agnostic training. *NeuroImage*, 220:117081, 2020.
- [51] Mingzhu Wang and Jack CP Cheng. A unified convolutional neural network integrated with conditional random field for pipe defect segmentation. *Computer-Aided Civil and Infrastructure Engineering*, 35(2):162–177, 2020.
- [52] Xide Xia and Brian Kulis. W-net: A deep model for fully unsupervised image segmentation. *arXiv preprint arXiv:1711.08506*, 2017.
- [53] Paul A. Yushkevich, Joseph Piven, Heather Cody Hazlett, Rachel Gimpel Smith, Sean Ho, James C. Gee, and Guido Gerig. User-guided 3D active contour segmentation of anatomical structures: Significantly improved efficiency and reliability. *NeuroImage*, 31(3):1116–1128, 2006.
- [54] Shuai Zheng, Sadeep Jayasumana, Bernardino Romera-Paredes, Vibhav Vineet, Zhizhong Su, Dalong Du, Chang Huang, and Philip HS Torr. Conditional random fields as recurrent neural networks. In *Proceedings of the IEEE international conference on computer vision*, pages 1529–1537, 2015.

EVC-Net: Supplement

Jong Sung Park

Department of Intelligent Systems Engineering
 Indiana University
 Bloomington, IN 47405
 jp109@iu.edu

Shreyas Fadnavis

Department of Intelligent Systems Engineering
 Indiana University
 Bloomington, IN 47405
 shf.adn@iu.edu

Eleftherios Garyfallidis

Department of Intelligent Systems Engineering
 Indiana University
 Bloomington, IN 47405
 elef@iu.edu

Training details

Learning rate of 0.01 was used with the Adam optimizer [?], as it gave better and faster results than Stochastic Gradient Descent. Negative dice coefficient was chosen as a loss function. Two Tesla V100 GPUs were used while training. Each model was trained for 18 epochs. The CRF hyperparameters were manually selected by searching for parameters with the best intuitive segmentation results. Specific values used were 100 for each of the kernel weights, with a value of 1 for θ_α , θ_γ and 4 for θ_β . This is very distinct from values used in Computer Vision, most likely due to the nature of the T1 MR images. Max iterations until convergence were set to 100. 3D dense CRF implementation provided in <https://github.com/HiLab-git/SimpleCRF> was used for the CRF step.

Minor changes to V-Net

The number of nodes is the same between our model and the original V-Net [?] per different scales of the encoder and decoder. However, there is a slight difference in kernel size which can be seen in the code provided. The reasoning behind this was the difference in the shape of the input tensor, since their model uses $128 \times 128 \times 64$ while we use $128 \times 128 \times 128$. We have also added dropout [?] and layer normalization [?]. Dropout has been proven to reduce overfitting problems, which is sensitive to limited number of data and possible bias within them. Normalization could be critical in solving gradient vanishing problems. In the computer vision literature, the most popular normalization technique is batch normalization [?]. This normalizes the features in the layers within the mini batch. However, this is not ideal for brain extraction since it is hard to use a big enough batch size due to memory constraints. Layer normalization is a good alternative, which normalizes the features within the layer. Lastly, ReLU instead of PReLU [?] was chosen as the activation function, as it gave more stable results in our tests. The exact architecture and its hyperparameters can be viewed in our code.

Experiment Settings All the experiments that do not need GPUs were done using Intel Core i7-6700 CPU with 16 Gigabytes of RAM. The deep learning models were run using two Tesla V100s. Most of the models were run with default parameters. BET[?] was done with a -R option, which corrects the center of mass through a repetitive process. This is known to improve the BET

results if there are a lot of non-brain tissues in the image. Brainy[?] was corrected by averaging the results of randomly rotated inputs, along with an additional post-processing step of selecting the largest connected segment in the image. Both options were recommended in the instructions.

Code

We provide a python implementation of our model. The deep learning architecture code was written using Tensorflow. The pre-trained models are also included with examples of how to test them.

<https://figshare.com/s/fb46d229c702a54abf7e>

Licenses

DIPY[?]: DIPY was used to view the load, save and view the segmentation results. DIPY has a BSD-3 License provided here: <https://github.com/dipy/dipy/blob/master/LICENSE>

Tensorflow[?]: Tensorflow provided a convenient way of creating a Deep Learning architecture. Tensorflow's Apache License is available in this link: <https://github.com/tensorflow/tensorflow/blob/master/LICENSE>

SimpleCRF: To implement the CRF portion of the model, SimpleCRF was utilized. The BSD-3 license can be viewed here: <https://github.com/HiLab-git/SimpleCRF/blob/master/LICENSE>

Other packages used in the code for various functions include Numpy, Scipy, Scikit-image, and Nibabel. Their licences are in the links provided below:

Numpy[?] (BSD-3) <https://github.com/numpy/numpy/blob/main/LICENSE.txt>

Scipy[?] (BSD-3) <https://github.com/scipy/scipy/blob/main/LICENSE.txt>

Scikit-image[?] (BSD-3) <https://github.com/scikit-image/scikit-image/blob/main/LICENSE.txt>

Nibabel[?] (MIT) <https://github.com/nipy/nibabel/blob/master/COPYING>

Difference between ground truths

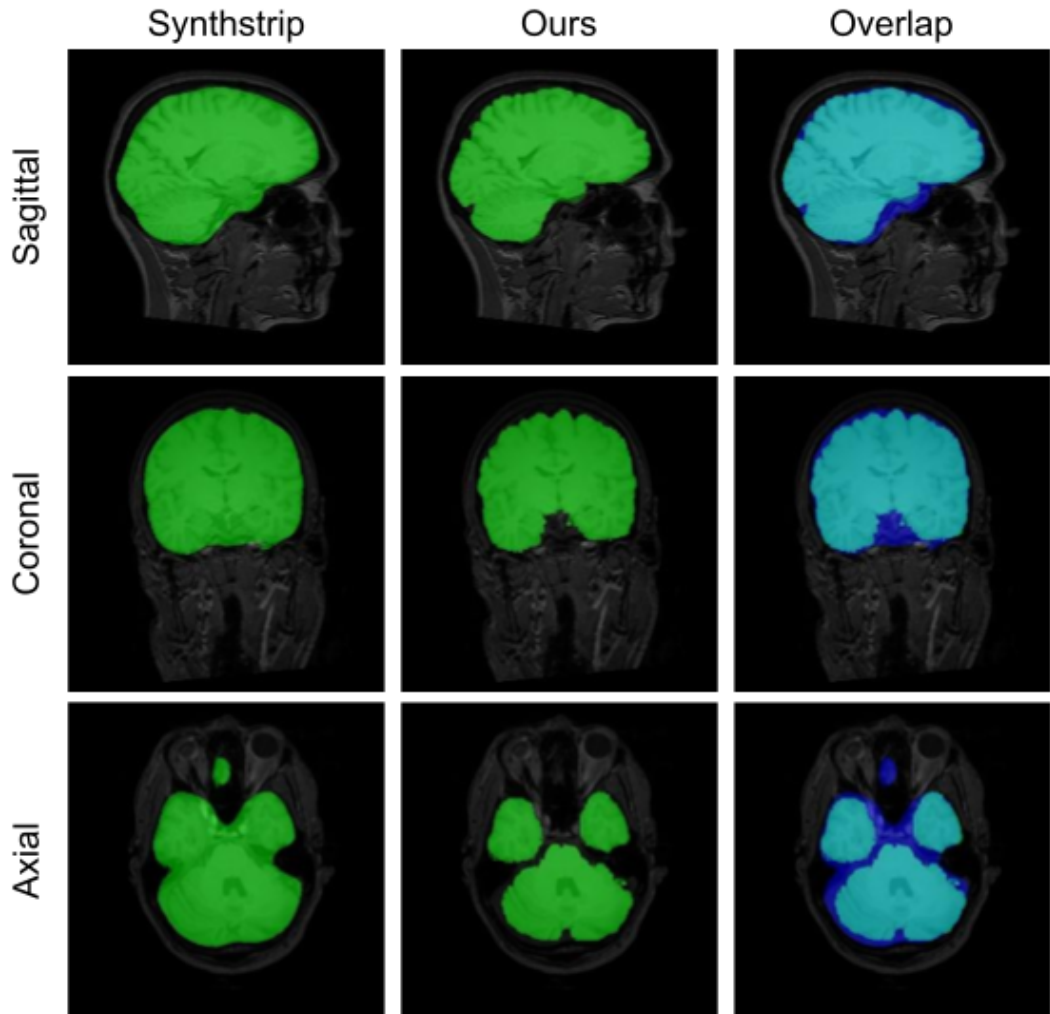


Figure 1: An overview of how the ground truth is different between our and Synthstrip’s [?] evaluation. The difference is clearly visible in the overlap. Note how our ground truth is completely within Synthstrip’s. This suggests that Synthstrip’s ground truth is a more smooth atlas based on reducing False Negatives, while ours is focused on the details on the borders of the brain. In the bottom row, green is our ground truth, blue is from Synthstrip and teal is the overlapping region.

Integrated Gradients

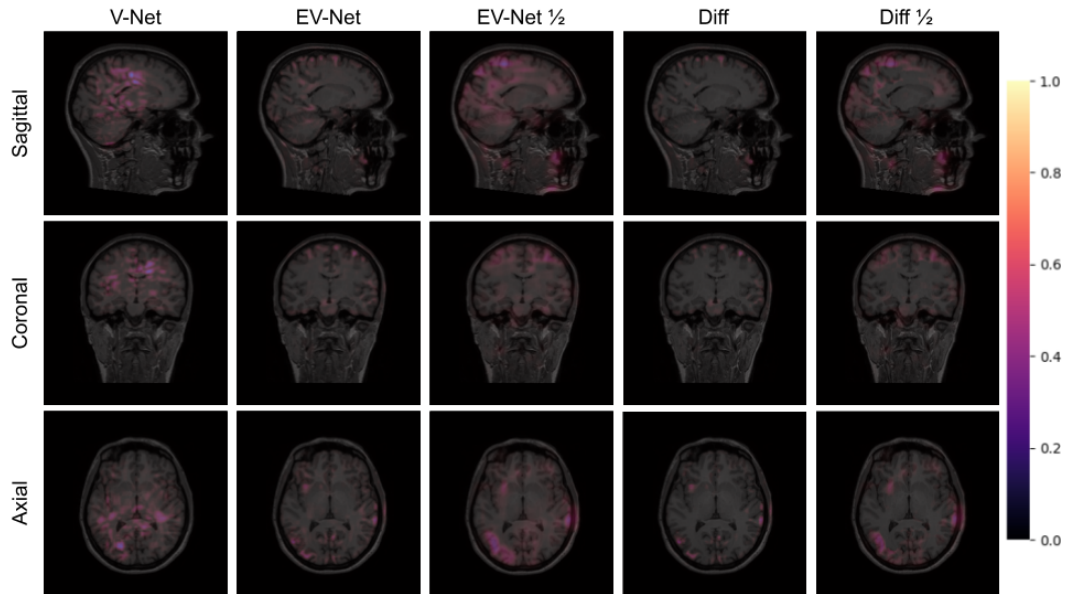


Figure 2: A figure of Integrated Gradients[?] comparisons between V-Net and EV-Net to show the difference in features considered in each of the models. The gradients were calculated using an all-zero array as baseline. The values were normalized for visualization. Differences show features that are important in EV-Net but considered at a minimum rate in V-Net. The fraction show the gradients based on lower scale inputs. For convenience, we have only included the one scale lower input. Important points to notice are how EV-Net considers more features important for a delicate segmentation of the brain than V-Net, and how the lower scale input's features are larger scale-wise than the original input.

Further comparisons

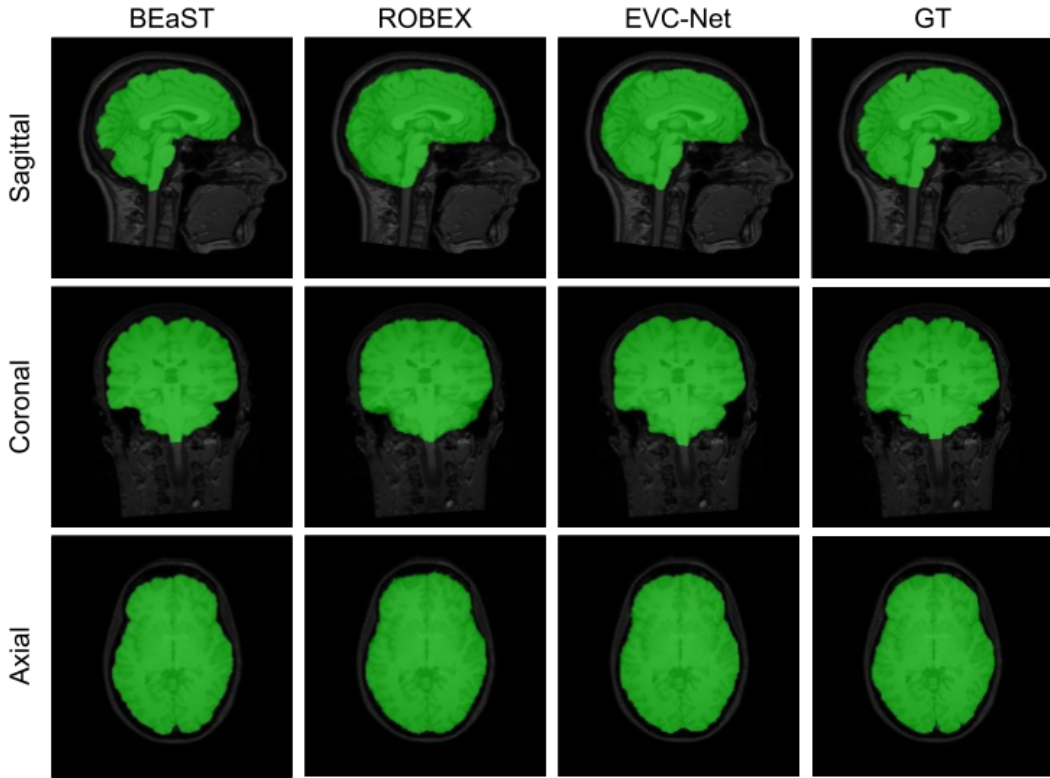


Figure 3: The figure shows some additional qualitative measures we did not include in the main paper due to spatial constraints. BEaST[?] manages to get good details, but is known to have some errors near the cerebellum, as shown in the top row. ROBEX[?] produces a smooth segmentation overall.